Supporting Information

Coagulation Factor XIIIa Inhibitor Tridegin: On the Role of Disulfide Bonds for Folding, Stability, and Function

Charlotte A. Bäuml,[†,#] Thomas Schmitz,[†,#] Ajay Abisheck Paul George,[†] Monica Sudarsanam,[†] Kornelia Hardes,[‡] Torsten Steinmetzer,[‡] Lori A. Holle,[§] Alisa S. Wolberg,[§] Bernd Pötzsch,[‖] Johannes Oldenburg,[‖] Arijit Biswas,[‖] and Diana Imhof*[†]

CONTENT

- 8 tables (Table S1-S8)
- 14 figures (Figures S1-S14)
- Supporting text

Table S1. Protecting group strategy and serine mutations used for the preparation of tridegin isomers.

Isomer	Connectivity	Trt[a]	Acm[a]	Ser-mutation
A[C19S,C25S]	C5-C17, C31-C37	C5-C17	C31-C37	S19-S25
B[C19S,C25S]	C5-C37, C17-C31	C5-C37	C17-C31	S19-S25
C[C19S,C25S]	C5-C31, C17-C37	C5-C31	C17-C37	S19-S25

[a]Protecting group used for the given Cys-pair.

Table S2. Analytical characterization of tridegin analogs produced in this study.

Peptide	t_R (C18) [min][a]	t_R (C8) [min][a]	$R_{f,}$[b]	[M + H]+ (calc.)[c]	[M + H]+ (meas.)[c]	Yield 1	Yield 2
A[C19S,C25S]	18.6	19.0	0.25	7746.9	7747.2	2 %[d]	14 %[e]
B[C19S,C25S]	18.5	19.0	0.25	7746.9	7746.9	5 %[d]	33 %[e]
C[C19S,C25S]	18.4	19.0	0.25	7746.9	7747.0	9 %[d]	19 %[e]
ABC[C19S,C25S]	19.2	18.6	-	7746.9	7746.9	20 %	-

t_R, retention time; $R_{f,1}$, $R_{f,2}$, TLC retention factor; calc., calculated.
[a]HPLC elution was carried out using a gradient of 20-50% acetonitrile containing 0.1% TFA (eluent B) in 30 min and 0.1% TFA in water (eluent A). [b]Water:butane:acetic acid:ethyl acetate (1/1/1/1), [c]average mass, [d]Work up: ascorbic acid. [e]Work up: extraction with ethyl acetate. The yield refers to the amount of linear precursor used for the oxidation process.

Table S3. Fragments found after chymotryptic digest of the linear precursors of isomers $A_{[C19S,C25S]}$-$C_{[C19S,C25S]}$.

Fragment	$[M + H]^+$ (calc.)[a]	$[M + H]^+$ (meas.)[a,b]	Cysteine protection
$A_{[C19S,C25S]}$			
KLLPC$_5$KEW	1016.54	1016.56	C$_5$(SH)
HQGIPNPRC$_{17}$W	1207.56	1207.59	C$_{17}$(SH)
C$_{31}$AF	411.20	411.18	C$_{31}$(Acm)
IPQC$_{37}$RPR	940.55	940.52	C$_{37}$(Acm)
$B_{[C19S,C25S]}$			
KLLPC$_5$KEW	1016.54	1016.57	C$_5$(SH)
C$_{17}$WSGADLESAQDQY	1643.70	1643.67	C$_{17}$(Acm)
C$_{31}$AF	411.20	411.18	C$_{31}$(Acm)
IPQC$_{37}$RPR	869.46	869.49	C$_{37}$(SH)
$C_{[C19S,C25S]}$			
KLLPC$_5$KEW	1016.54	1016.56	C$_5$(SH)
HQGIPNPRC$_{17}$W	1278.65	1278.62	C$_{17}$(Acm)
C$_{31}$AF	340.11	340.13	C$_{31}$(SH)
IPQC$_{37}$RPR	940.55	940.52	C$_{37}$(Acm)

[a]monoisotopic mass, [b]if the peptide was detected in a higher charged state, $[M + H]^+$ was calculated from this peak.

Table S4. Fragments found after chymotryptic digest of isomer $A_{[C19S, C25S]}$.

Fragment	$[M + H]^+$ (calc.)[a]	$[M + H]^+$ (meas.)[a,b]	Disulfide bridge
$C_{31}AF$ $C_{37}RPR$	868.41	868.38	C_{31}-C_{37}
$C_{31}AF$ $C_{37}RPRSEL$	1197.57	1197.55	C_{31}-C_{37}
$C_{31}AF$ $IPQC_{37}RPR$	1206.59	1206.59	C_{31}-C_{37}
$C_{31}AF$ $IPQC_{37}RPRSEL$	1535.75	1535.74	C_{31}-C_{37}
$C_{31}AF$ $IPQC_{37}RPRSELIKPM$	2005.02	2005.03	C_{31}-C_{37}
$KLLPC_5KEW$ $C_{17}W$	1321.63	1321.67	C_5-C_{17}
$KLLPC_5KEW$ $C_{17}WSGADLESAQDQY$	2586.15	2586.15	C_5-C_{17}

[a]monoisotopic mass, [b]if the peptide was detected in a higher charged state, $[M + H]^+$ was calculated from this peak.

Table S5. Fragments found after chymotryptic digest of peptide $ABC_{[C19S,C25S]}$.

Fragment	$[M + H]^+$ (calc.)[a]	$[M + H]^+$ (meas.)[a,b]	Disulfide bridge (isomer)
$KLLPC_5KEW$ $C_{17}W$	1321.64	1321.67	C_5-C_{17} ($A_{[C19S,C25S]}$)
$C_{31}AF$ $IPQC_{37}RPR$	1206.59	1206.60	C_{31}-C_{37} ($A_{[C19S,C25S]}$)
$KLLPC_5KEW$ $PQC_{37}RPR$	1769.93	1769.96	C_5-C_{37} ($B_{[C19S,C25S]}$)
$C_{17}W$ $C_{31}AF$	645.22	645.20	C_{17}-C_{31} ($B_{[C19S,C25S]}$)
$KLLPC_{05}KEW$ $C_{31}AF$	1353.67	1353.69	C_5-C_{31} ($C_{[C19S,C25S]}$)
$C_{17}W$ $C_{37}RPR$	836.37	836.37	C_{17}-C_{37} ($C_{[C19S,C25S]}$)

[a]monoisotopic mass, [b]if the peptide was detected in a higher charged state, $[M + H]^+$ was calculated from this peak.

Table S6: Statistical data obtained for IC_{50} comparison in the fluorogenic FXIIIa assay and in the whole blood clot contraction assay.

Peptide 1	Mean 1	Peptide 2	Mean 2	Diff.	SE of diff.	t ratio	df	Adjusted P value
Fluorogenic FXIIIa assay								
ABC	0.45	**A[C19S,C25S]**	0.55	0.10	0.0306	3.266	5	0.0223 *
ABC	0.45	**B[C19S,C25S]**	0.50	0.05	0.0307	1.625	4	0.1787
ABC	0.45	**C[C19S,C25S]**	0.48	0.03	0.0356	0.842	5	0.4382
ABC	0.45	**ABC[C19S,C25S]**	0.51	0.06	0.0188	3.199	3	0.0494 *
ABC	0.45	**All-Ser**	0.72	0.27	0.0300	8.996	5	0.0003 ***
A[C19S,C25S]	0.55	**B[C19S,C25S]**	0.50	0.05	0.0367	1.362	5	0.2315
A[C19S,C25S]	0.55	**C[C19S,C25S]**	0.48	0.07	0.0374	1.872	6	0.1104
B[C19S,C25S]	0.50	**C[C19S,C25S]**	0.48	0.02	0.0410	0.488	5	0.6463
Whole blood clot contraction assay								
A[C19S,C25S]	0.7	**B[C19S,C25S]**	1.1	0.4	0.238	1.680	4	0.1682
A[C19S,C25S]	0.7	**C[C19S,C25S]**	2.3	1.6	1.291	1.239	4	0.2830
B[C19S,C25S]	1.1	**C[C19S,C25S]**	2.3	1.2	1.271	0.944	4	0.3987

Diff., difference; SE, standard error, df, degrees of freedom. * $P < 0.05$; ** $P < 0.01$; *** $P < 0.001$
Statistical significance determined using the Holm-Sidak method. Each row was analyzed individually without using a consistent standard deviation. P values less than 0.01 were considered statistically significant.

Table S7: Summary of determined IC_{50} values for tested peptides.

Peptide	Fluorogenic FXIIIa assay		Whole blood clotting assay	
	IC_{50}	SD	IC_{50}	SD
$A_{[C19S,C25S]}$	0.55 µM	± 0.05 µM	0.7 µM	± 0.4 µM
$B_{[C19S,C25S]}$	0.50 µM	± 0.05 µM	1.1 µM	± 0.1 µM
$C_{[C19S,C25S]}$	0.48 µM	± 0.06 µM	2.3 µM	± 2.2 µM
$ABC_{[C19S,C25S]}$	0.51 µM	± 0.02 µM	n. d.	n. d.
All-Ser	0.72 µM	± 0.05 µM	n. d.	n. d.
ABC	0.45 µM	± 0.03 µM	n. d.	n. d.
$P_{39}-P_{64}$	n. d.	n. d.	2.2 µM	± 2.0 µM

SD, standard deviation; n.d., not determined.

Table S8. Average RMSD values of the isomers in the 300 ns MD simulation.

Isomer	RMSD of whole molecule (Å)	RMSD of N-terminal residues 1-37 (Å)	RMSD of C-terminal residues 38-66 (Å)
A	3.331	2.357	3.939
A*	2.805	2.147	2.597
$A_{[C19S,C25S]}$	2.589	1.171	2.925
B	2.704	1.768	3.024
B*	3.102	1.425	3.928
$B_{[C19S,C25S]}$	10.747	1.539	8.250
C	1.707	1.544	1.682
C*	2.462	2.276	1.622
$C_{[C19S,C25S]}$	7.033	2.634	6.524

*Isomers with *in silico* opened $C_{19}-C_{25}$ disulfide bond yielding two SH-groups.
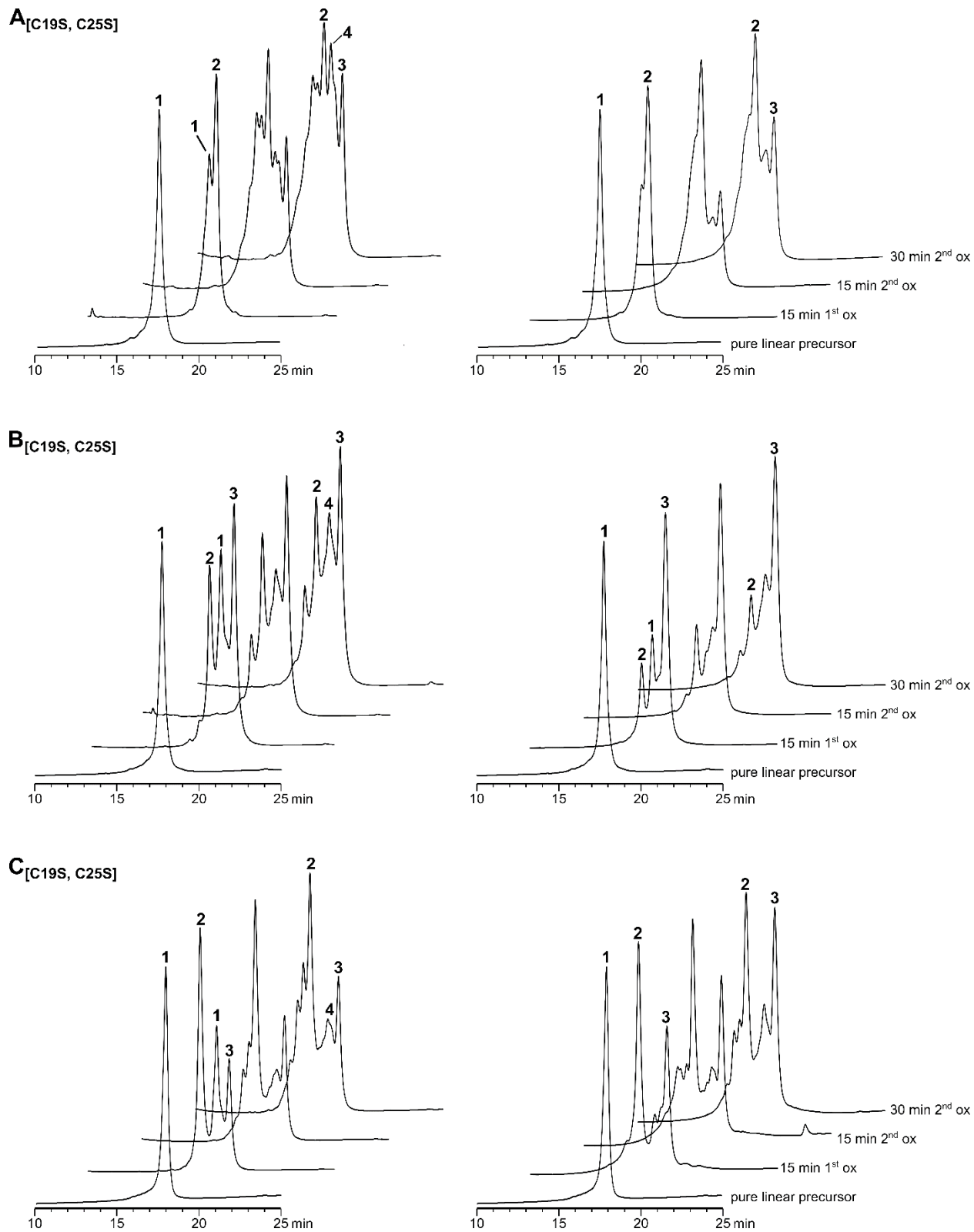
Figure S1. 1st and 2nd Oxidation of peptides **A$_{[C19S,C25S]}$** - **C$_{[C19S,C25S]}$**. Reaction progress: Oxidation strategy stopped using ascorbic acid (left) or by extraction of iodine with ethyl acetate

(right). More details are described in the Experimental section (Oxidation of linear precursor peptides). The HPLC elution was performed using a gradient of 20-50% eluent B, which was 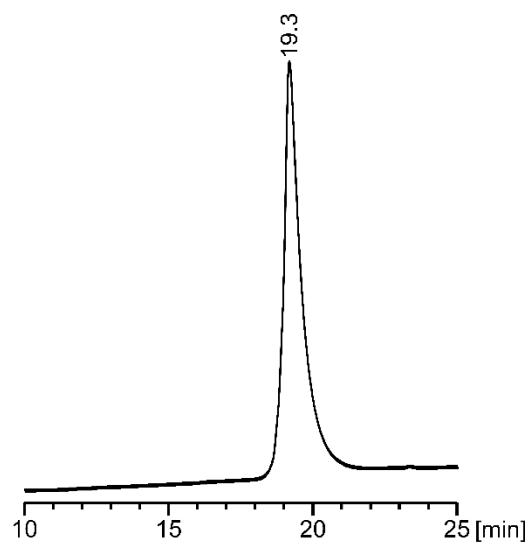0.1% TFA in acetonitrile (eluent A: 0.1% TFA in water) in 30 min. 1: linear precursor containing 2 Acm-protected Cys residues; 2: peptide with first disulfide bridge closed and 2 Acm-protected Cys residues; 3: $A_{[C19S,C25S]}$, $B_{[C19S,C25S]}$, and $C_{[C19S,C25S]}$, respectively; 4: unidentified byproducts.
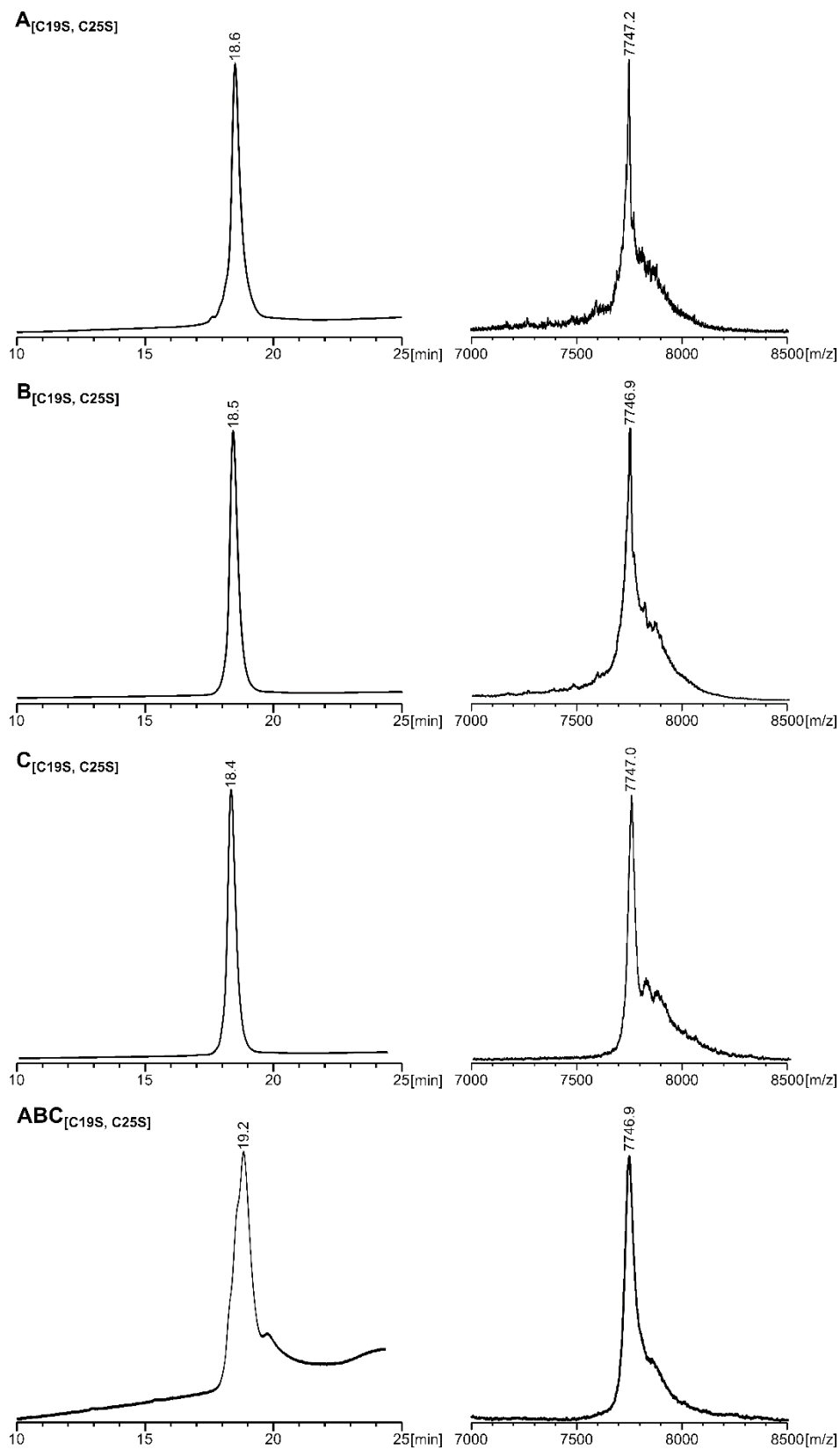
Figure S2. HPLC profiles (left) of purified tridegin analogs **A**[C19S,C25S] - **C**[C19S,C25S] and

ABC[C19S,C25S] as well as corresponding MALDI-TOF mass spectra (right). The HPLC elution was performed using a gradient of 20-50% eluent B, which was 0.1% TFA in acetonitrile (eluent A: 0.1% TFA in water) in 30 min.

Figure S3. HPLC co-elution profile of the purified tridegin analogs ($A_{[C19S,C25S]}$ - $C_{[C19S,C25S]}$) in an equimolar mixture on a C18 column. The HPLC elution was performed using a gradient of 20-50% eluent B, which was 0.1% TFA in acetonitrile (eluent A: 0.1% TFA in water) in 30 min.
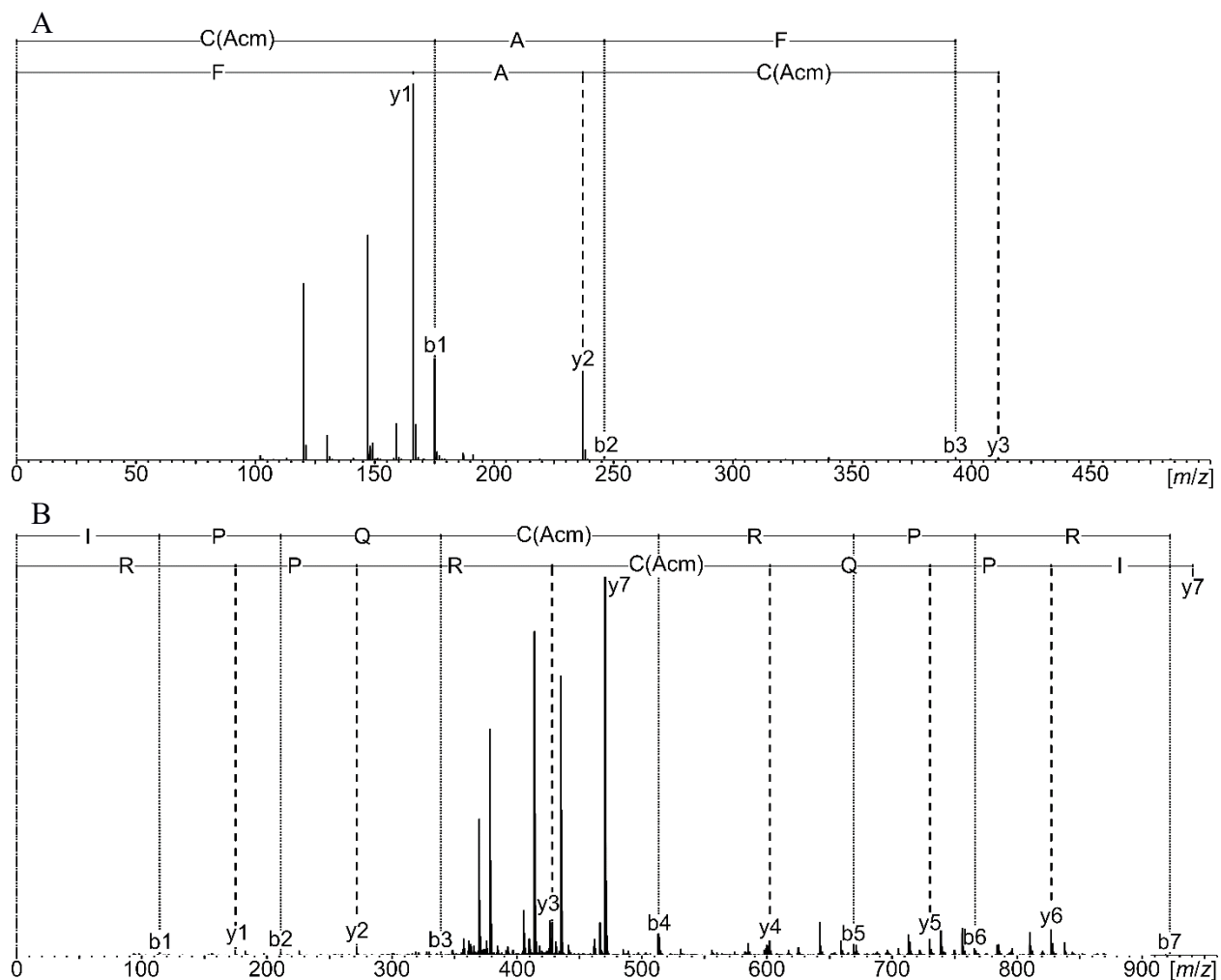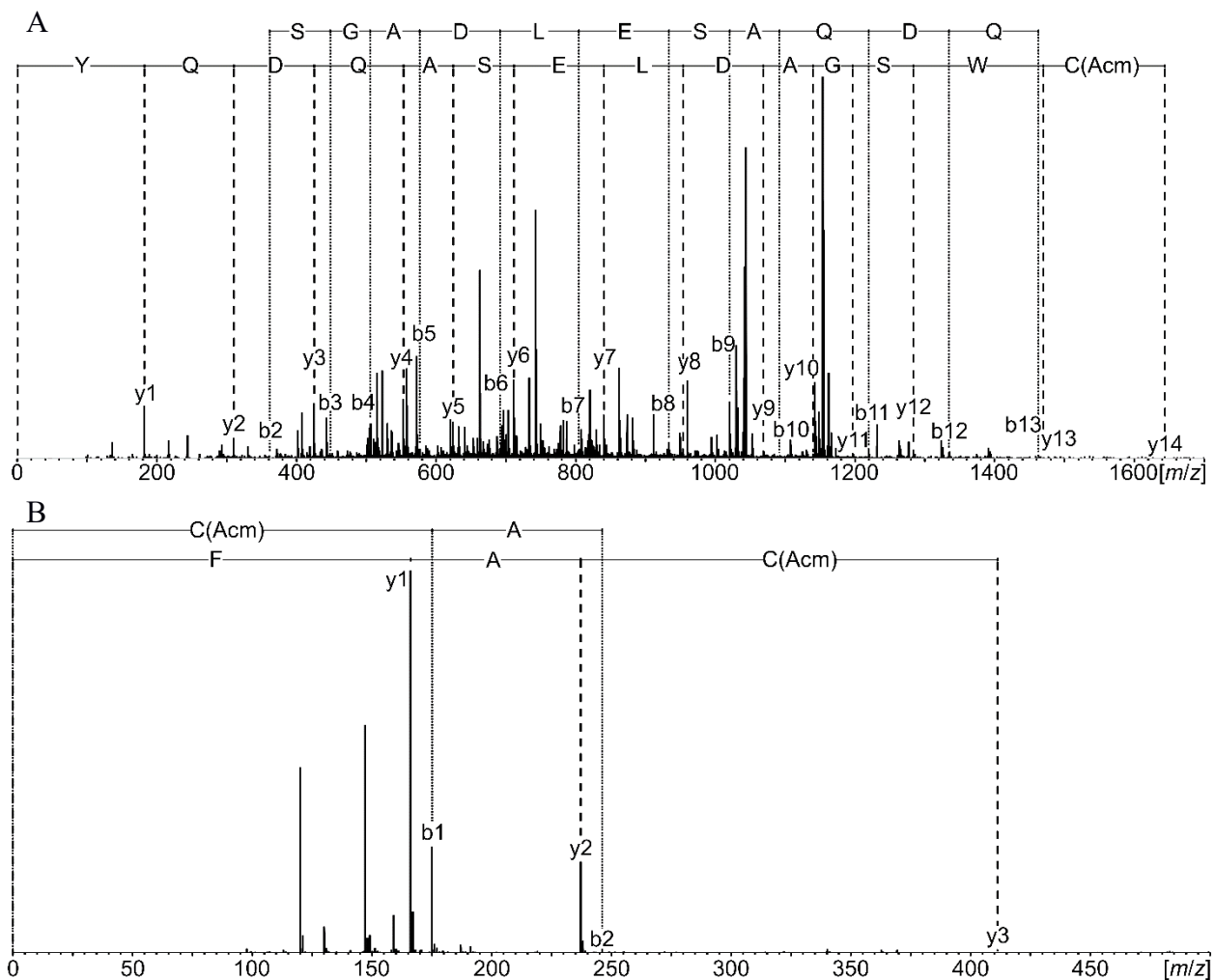
Figure S4. Sequence analysis of the digested linear precursor of **A[C19S,C25S]** with two protected cysteines on position 31 and 37 via tandem mass spectrometry. Chymotryptic digest of the linear precursor was performed and the digested fragments were analyzed by subsequent tandem mass spectrometry to check the correct positions of the Acm-protected cysteines. **A)** Determination of the Acm-protected C_{31} by sequence analysis of the fragment $C_{31}AF$. **B)** Determination of the Acm-protected C_{37} by sequence analysis of the fragment $IPQC_{37}RPR$.
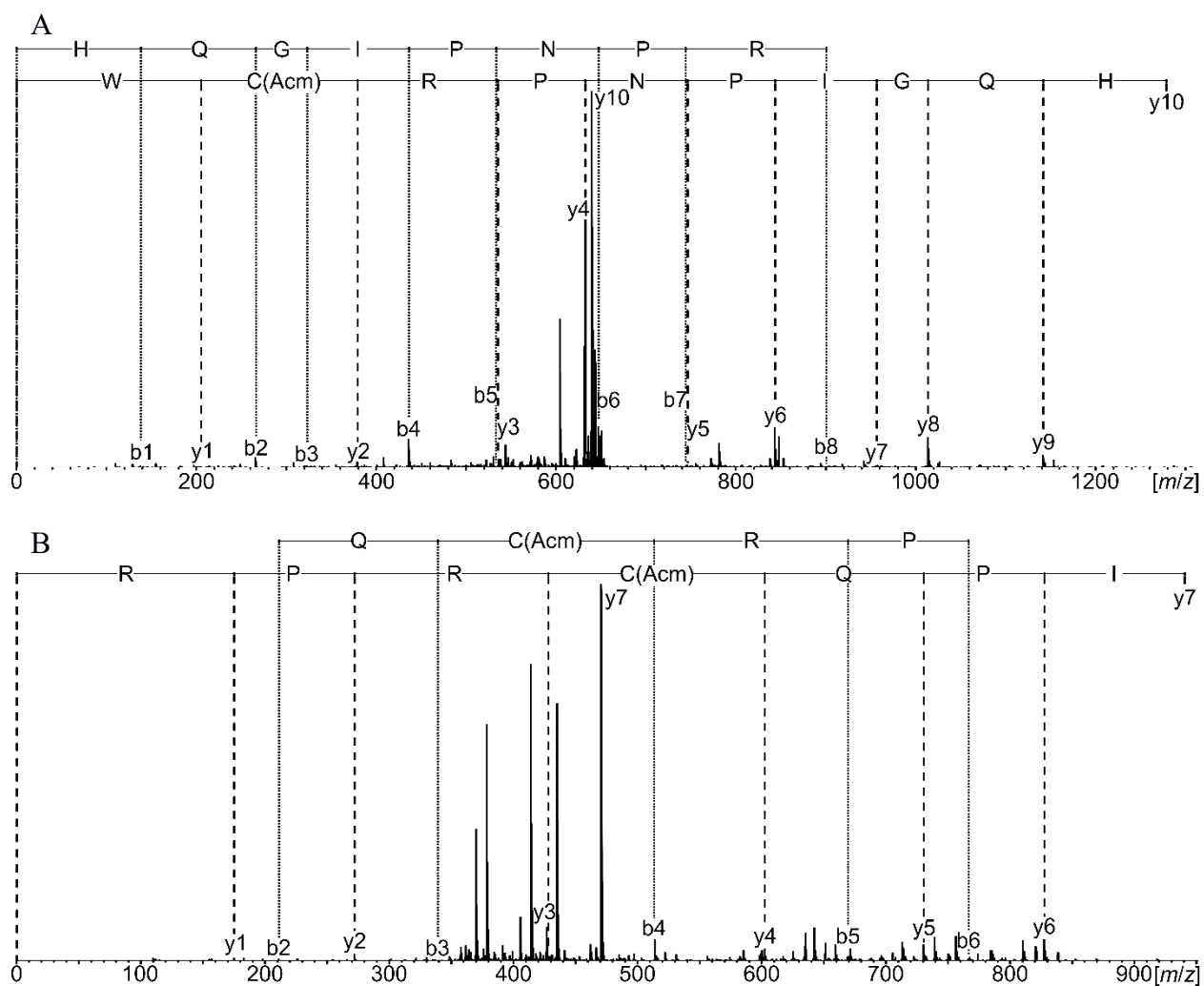
Figure S5. Sequence analysis of the digested linear precursor of $B_{[C19S, C25S]}$ with two protected cysteines on position 17 and 31 via tandem mass spectrometry. Chymotryptic digest of the linear precursor was performed and the digested fragments were analyzed by subsequent tandem mass spectrometry to check the correct positions of the Acm-protected cysteines. **A)** Determination of the Acm-protected C_{17} by sequence analysis of the fragment C_{17}WSGADLESAQDQY. **B)** Determination of the Acm-protected C_{31} by sequence analysis of the fragment C_{31}AF.

Figure S6. Sequence analysis of the digested linear precursor of $C_{[C19S,C25S]}$ with two protected

cysteines on position 17 and 37 via tandem mass spectrometry. Chymotryptic digest of the linear

precursor was performed and the digested fragments were analyzed by subsequent tandem mass

spectrometry to check the correct positions of the Acm-protected cysteines. **A)** Determination of

the Acm-protected C_{17} by sequence analysis of the fragment $HQGIPNPRC_{17}W$. **B)**

Determination of the Acm-protected C_{37} by sequence analysis of the fragment $IPQC_{37}RPR$.
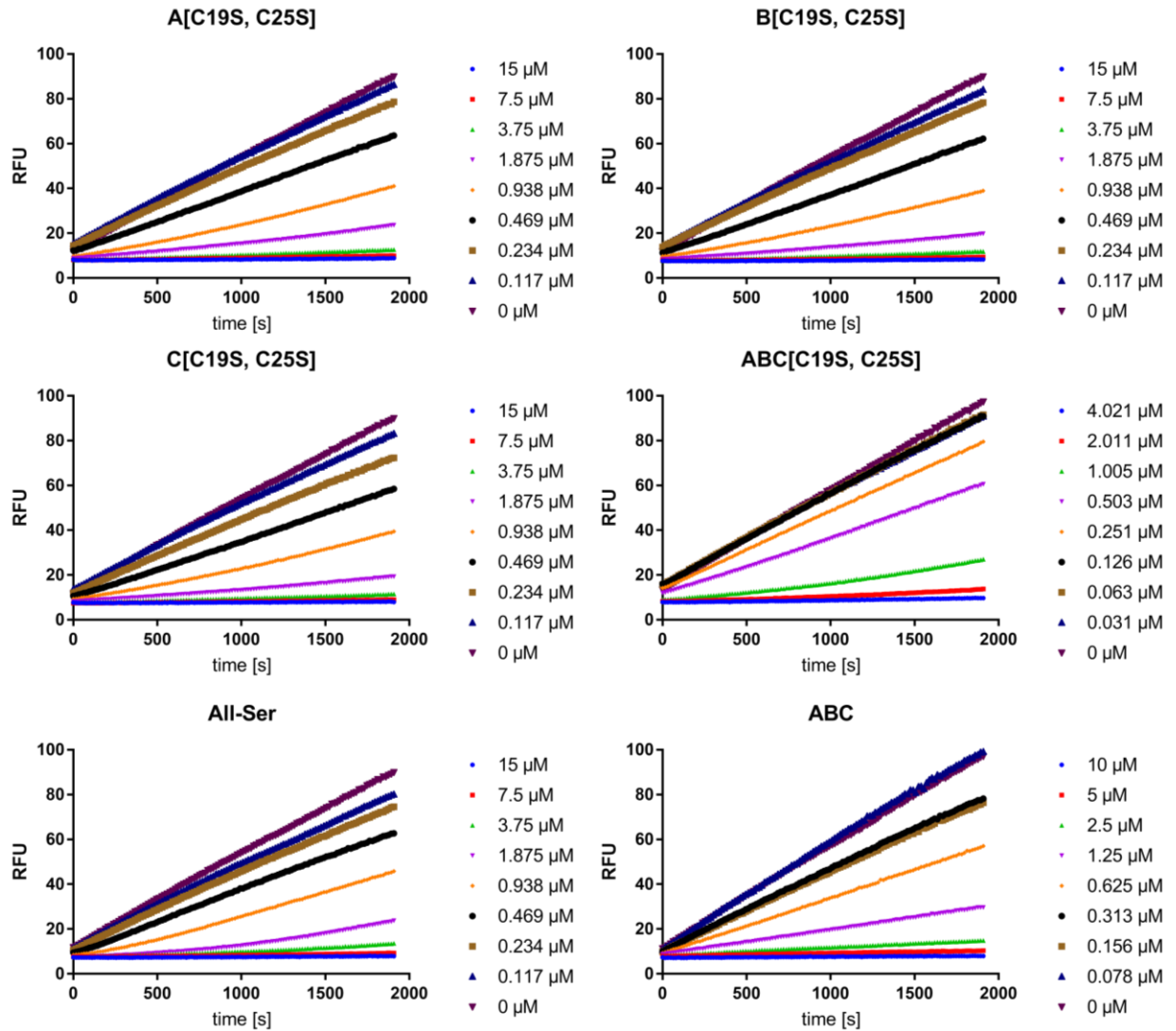
Figure S7: Fluorogenic FXIIIa assay in the presence of inhibitors **A[C19S,C25S]**, **B[C19S,C25S]**, **C[C19S,C25S]**, **ABC[C19S,C25S]**, **All-Ser**, and **ABC**. All inhibitors are stable inhibitors. Substrate-like behavior, i.e. competition with the fluorogenic substrate in the beginning and subsequent loss of inhibitory function, is not observed.
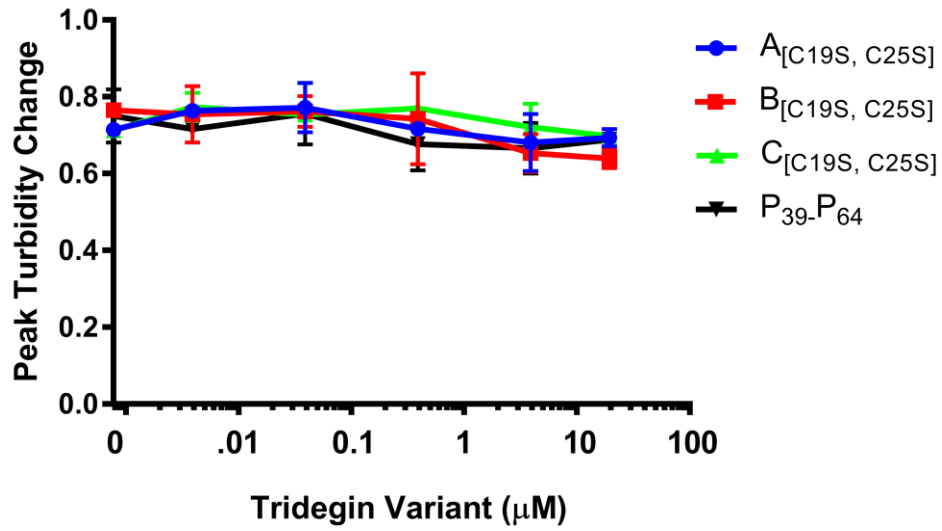
Figure S8: Peak turbidity change of plasma treated with various concentrations of tridegin variants and then clotted by recalcification and addition of tissue factor.
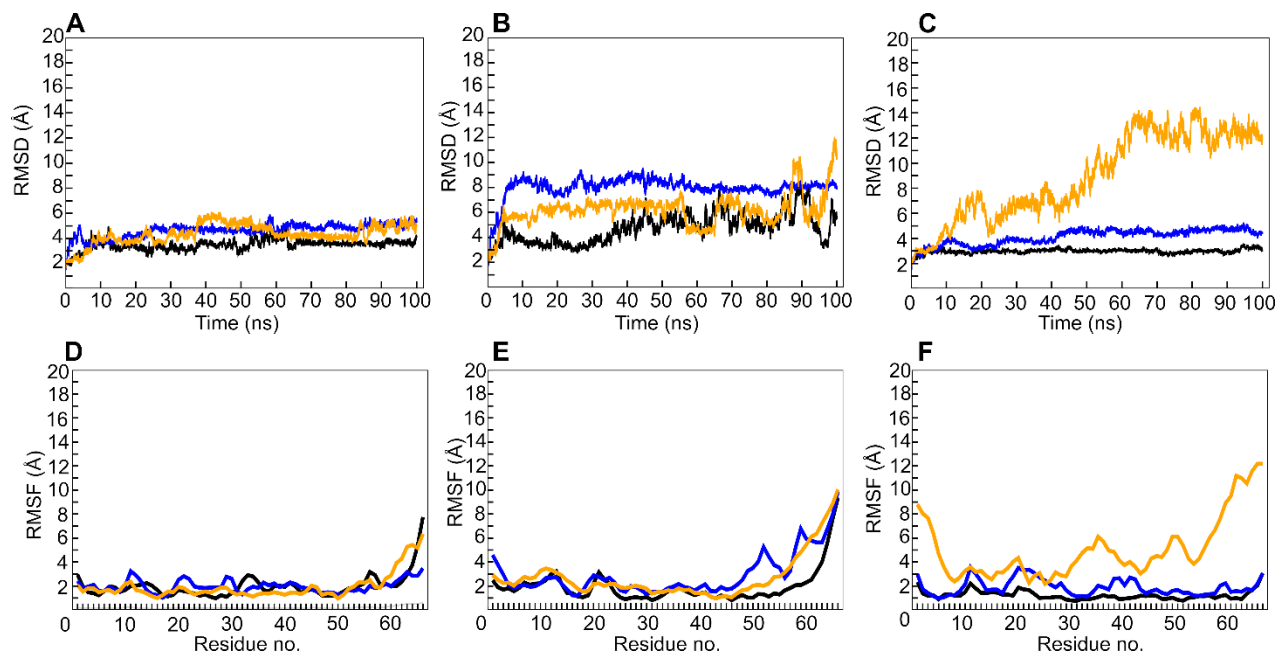
Figure S9. Backbone RMSD and RMSF profiles from the 100 ns MD simulations of the tridegin isomers and their variants. **A)** Overlay of RMSD profile of Isomer **A** (black), Isomer **A** with *in silico* removal of the C_{19}-C_{25} disulfide bond (blue), and the analog **A**$_{[C19S,C25S]}$ (orange). **B)** Overlay of RMSD profile of Isomer **B** (black), Isomer **B** with *in silico* removal of the C_{19}-C_{25} disulfide bond (blue), and the analog **B**$_{[C19S,C25S]}$ (orange). **C)** Overlay of RMSD profile of Isomer **C** (black), Isomer **C** with *in silico* removal of the C_{19}-C_{25} disulfide bond (blue) and the analog **C**$_{[C19S,C25S]}$ (orange). **D)** Overlay of RMSF profile of Isomer **A** (black), Isomer **A** with *in silico* removal of the C_{19}-C_{25} disulfide bond (blue), and the analog **A**$_{[C19S,C25S]}$ (orange). **E)** Overlay of RMSF profile of Isomer **B** (black), Isomer **B** with *in silico* removal of the C_{19}-C_{25} disulfide bond (blue), and the analog **B**$_{[C19S, C25S]}$ (orange). **F)** Overlay of RMSF profile of Isomer **C** (black), Isomer **C** with *in silico* removal of the C_{19}-C_{25} disulfide bond (blue), and the analog **C**$_{[C19S,C25S]}$ (orange).
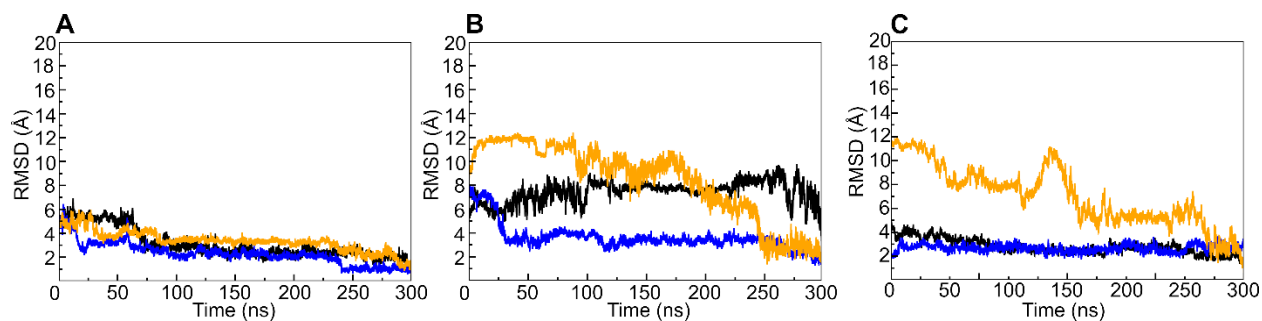
Figure S10. Backbone RMSD profiles from the 300 ns MD simulations of the tridegin isomers and their variants. **A)** Overlay of RMSD profile of Isomer **A** (black), Isomer **A** with *in silico* removal of the C_{19}-C_{25} disulfide bond (blue), and the analog **A[C19S,C25S]** (orange). **B)** Overlay of RMSD profile of Isomer **B** (black), Isomer **B** with *in silico* removal of the C_{19}-C_{25} disulfide bond (blue), and the analog **B[C19S,C25S]** (orange). **C)** Overlay of RMSD profile of Isomer **C** (black), Isomer **C** with *in silico* removal of the C_{19}-C_{25} disulfide bond (blue) and the analog **C[C19S,C25S]** (orange).
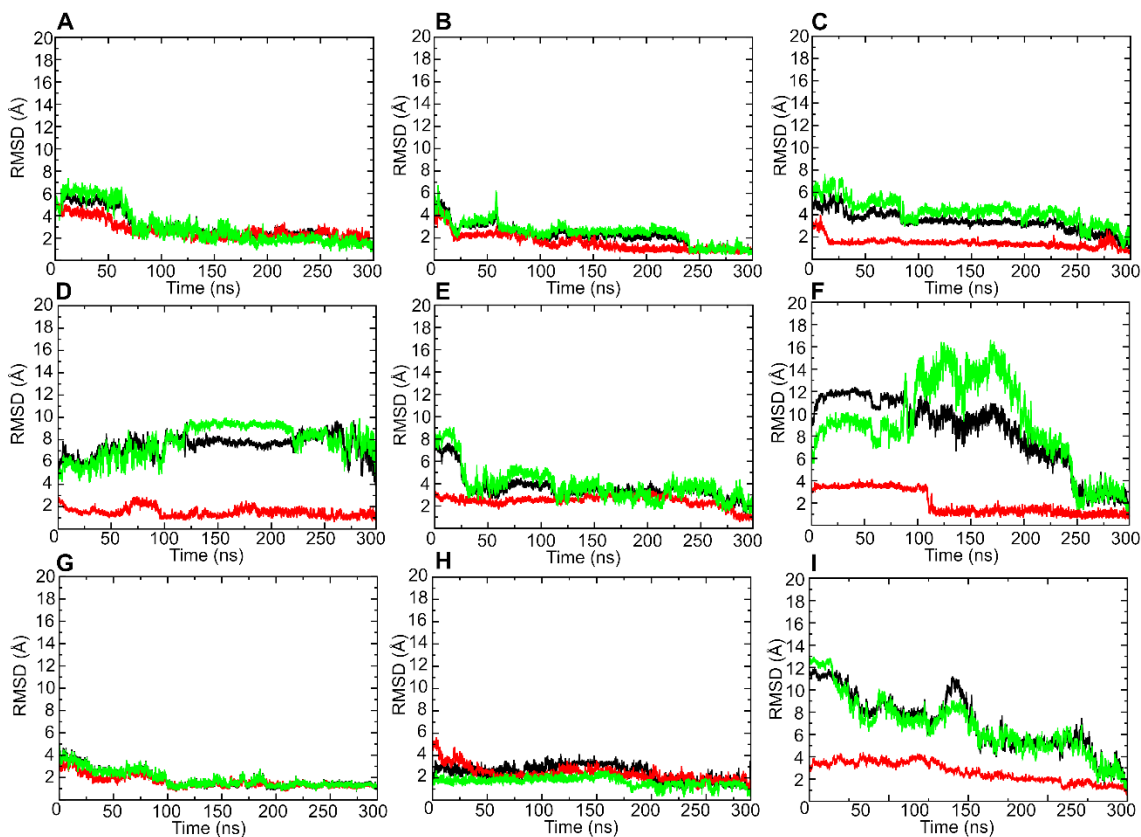
Figure S11. Backbone RMSD profiles from the 300 ns MD simulations of the tridegin isomers and their variants. **A)** Isomer **A**. **B)** Isomer **A** with *in silico* removal of the C_{19}-C_{25} disulfide bond. **C)** Analog **A**[C19S,C25S]. **D)** Isomer **B**. **E)** Isomer **B** with *in silico* removal of the C_{19}-C_{25} disulfide bond. **F)** Analog **B**[C19S,C25S]. **G)** Isomer **C**. **H)** Isomer **C** with *in silico* removal of the C_{19}-C_{25} disulfide bond. **I)** Analog **C**[C19S,C25S]. In all the panels spanning from A to I the black trace represents the backbone RMSD of the full molecule, the red trace represents the RMSD contribution of the N-terminal disulfide bonded residues 1-37 and the green trace represents the RMSD contribution of the flexible C-terminal residues 38-66.
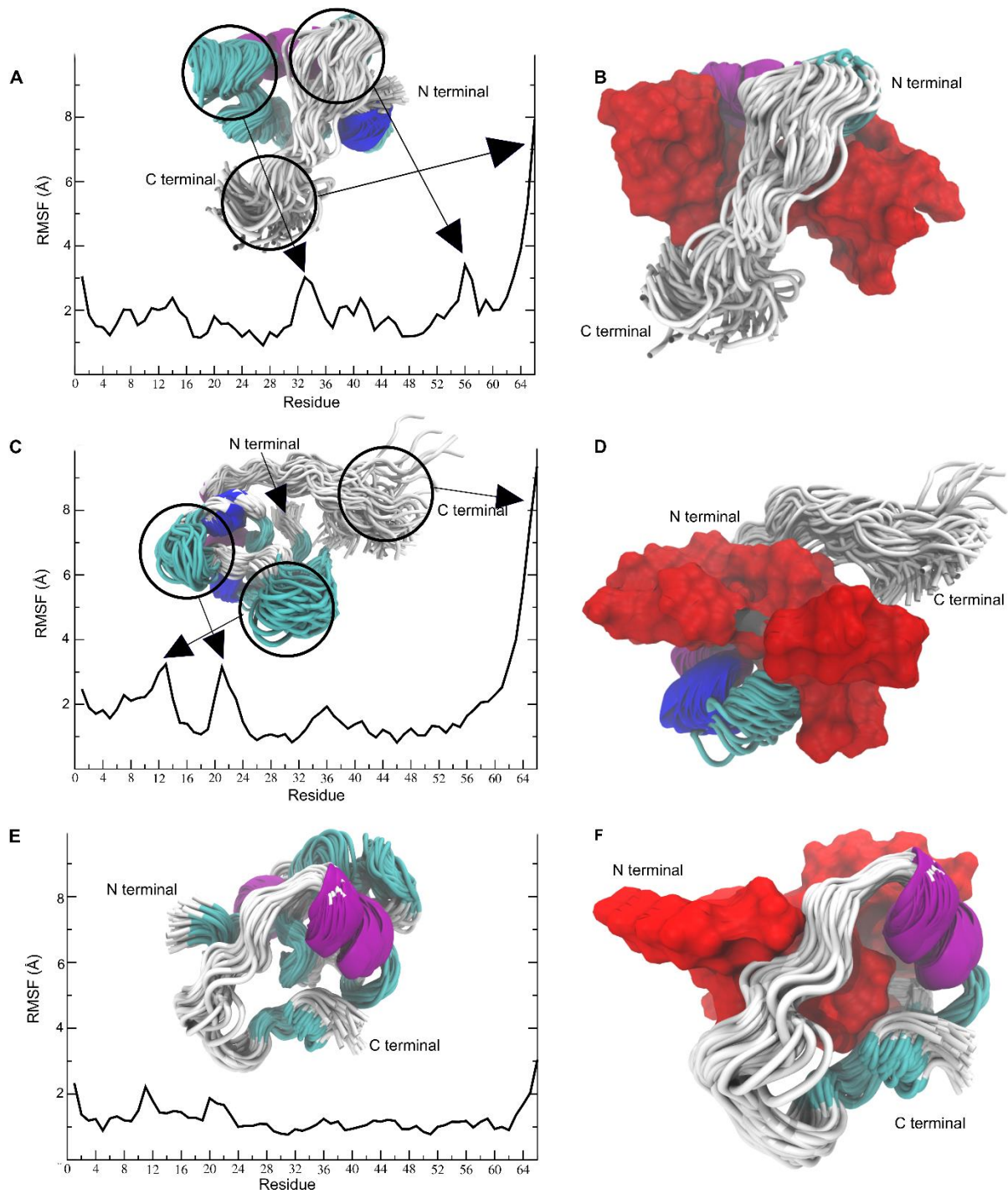
Figure S12. Conformational flexibility of isomers **A**, **B**, and **C** in simulation. **A)** Representation of the conformational flexibility of **A** with a cartoon representation of 100 snapshots with secondary structures distinguished (coil – white, turn – cyan, α-helix – purple, and 3_10 helix –

blue) from the MD simulation of the peptide. Regions of pronounced flexibility are highlighted by black circles with arrows leading to the corresponding points on the RMSF plot of the individual residues from the simulation. **B) A** with residues 1-37 represented as surface (red) and 100 superimposed snapshots of the residues 38-66 shown as cartoons to clearly distinguish the disulfide bound and unbound parts of the peptide. **C)** Representation of the conformational flexibility of **B** with a cartoon representation of 100 snapshots with secondary structures distinguished (coil – white, turn – cyan, α-helix – purple, and 3_10 helix – blue) from the MD simulation of the peptide. Regions of pronounced flexibility are highlighted by black circles with arrows leading to the corresponding points on the RMSF plot of the individual residues from the simulation. **D) B** with residues 1-37 represented as surface (red) and 100 superimposed snapshots of the residues 38-66 shown as cartoons to clearly distinguish the disulfide bound and unbound parts of the peptide. **E)** Representation of the conformational flexibility of **C** with a cartoon representation of 100 snapshots with secondary structures distinguished (coil – white, turn – cyan and α-helix – purple) from the MD simulation of the peptide. No distinct regions of flexibility are marked due to the absence of any and the RMSF plot shown below provides justification for the same. **F) C** with residues 1-37 represented as surface (red) and 100 superimposed snapshots of the residues 38-66 shown as cartoons to clearly distinguish the disulfide bound and unbound parts of the peptide.
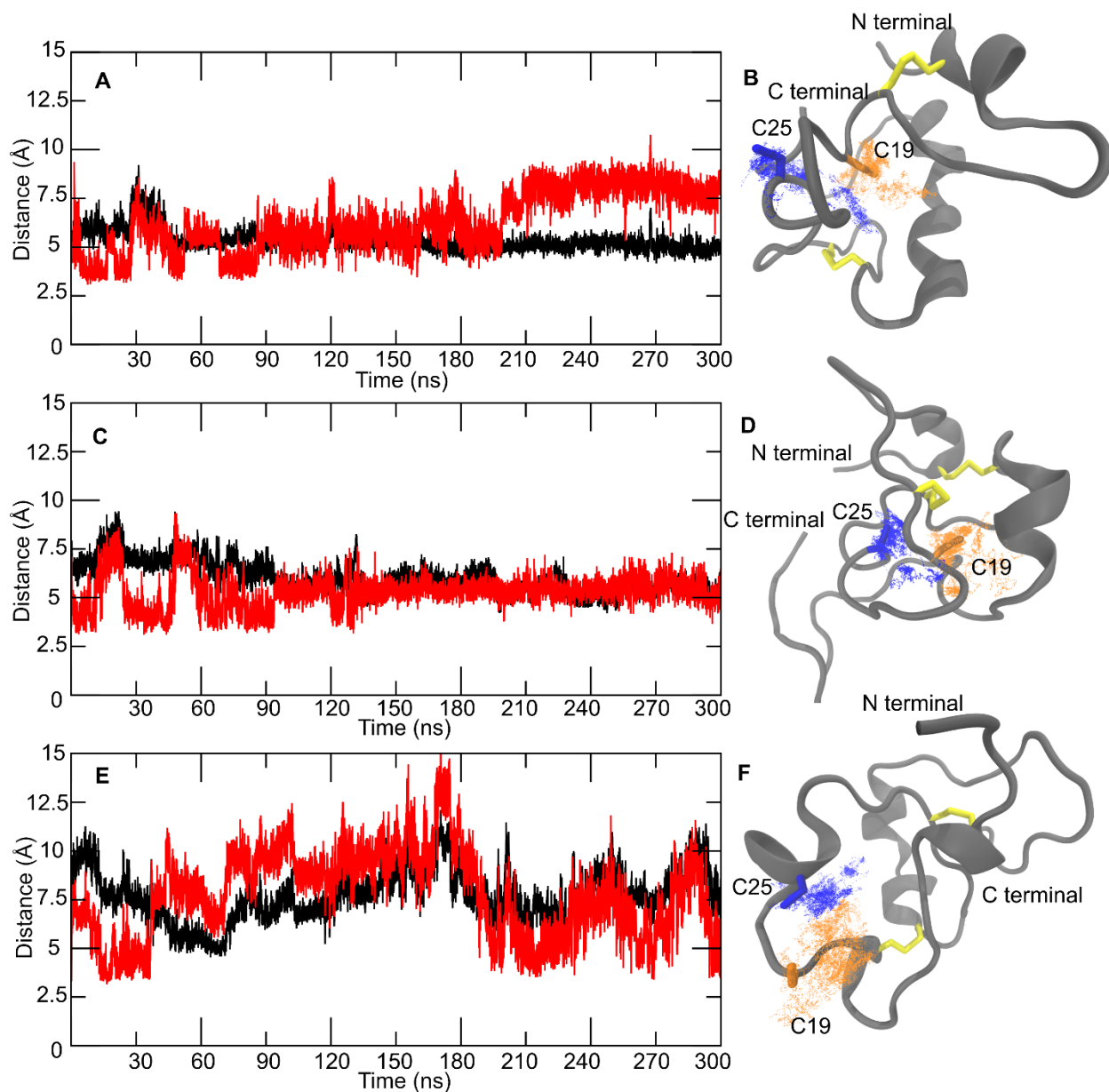
Figure S13. Evolution of S_γ and C_α distances between the unbound C_{19} and C_{25} residues after *in silico* removal of the C_{19}-C_{25} disulfide bond. **A)** Distances between the S_γ (red trace) and C_α (black trace) atoms of C_{19} and C_{25} for isomer **A** over the 300 ns. **B)** The simulation starting structure of isomer **A** (gray cartoon) with the unbound C_{19} (orange stick) and C_{25} (blue stick). 10000 conformations relative to the starting structure sampled by the S_γ atom of C_{19} is represented by orange dots while the same for the C_{25} residue is shown by blue dots. **C)**

Distances between the S_γ (red trace) and C_α (black trace) atoms of C_{19} and C_{25} for isomer **B** over the 300 ns. **D)** The simulation starting structure of isomer **B** (gray cartoon) with the unbound C_{19} (orange stick) and C_{25} (blue stick). 10000 conformations relative to the starting structure sampled by the S_γ atom of C_{19} is represented by orange dots while the same for the C_{25} residue is shown by blue dots. **E)** Distances between the S_γ (red trace) and C_α (black trace) atoms of C_{19} and C_{25} for isomer **C** over the 300 ns. **F)** The simulation starting structure of isomer **C** (gray cartoon) with the unbound C_{19} (orange stick) and C_{25} (blue stick). 10000 conformations relative to the starting structure sampled by the S_γ atom of C_{19} is represented by orange dots while the same for the C_{25} residue is shown by blue dots.
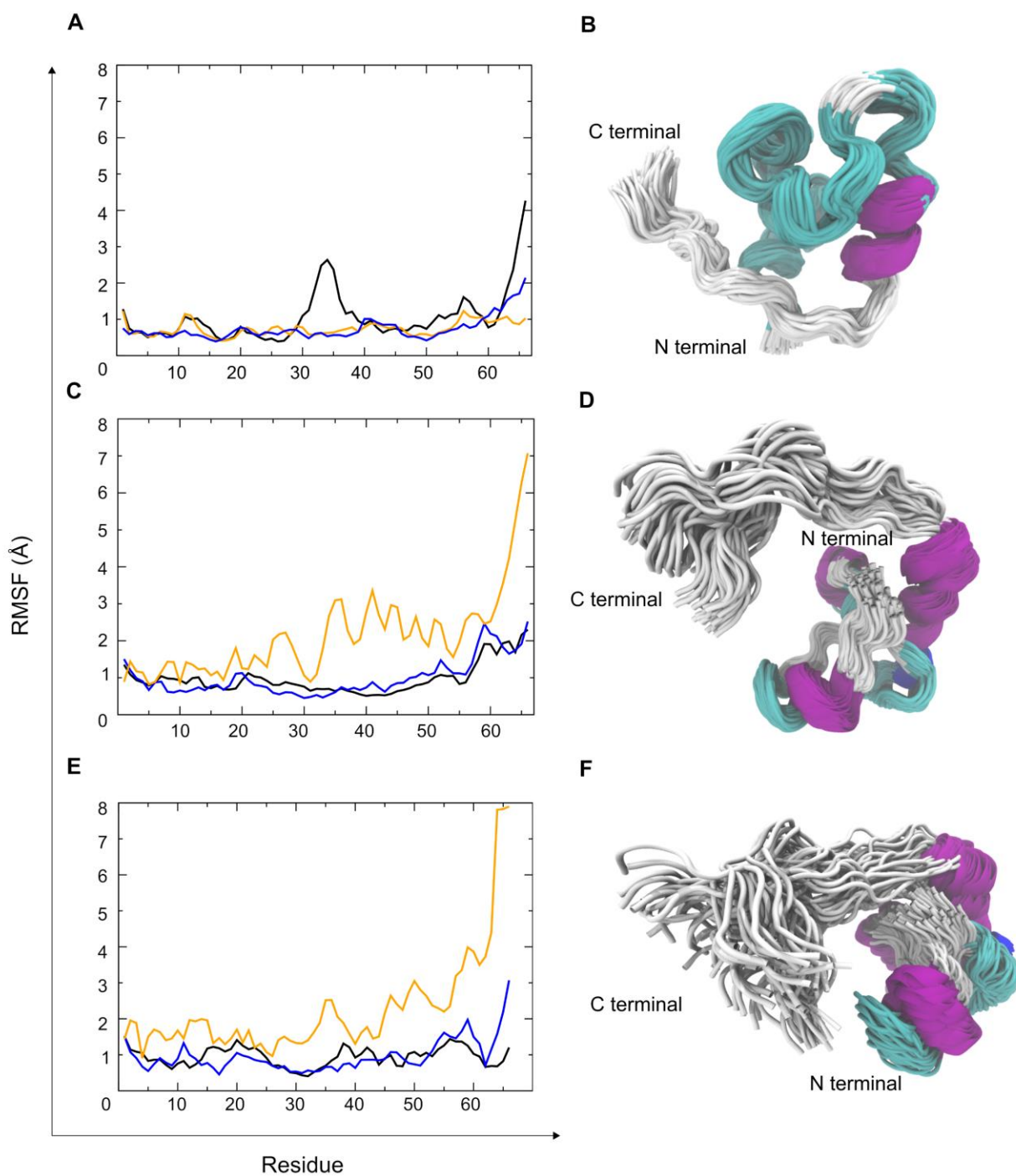
Figure S14. Conformational flexibility of isomers **A**[C19S,C25S], **B**[C19S,C25S], and **C**[C19S,C25S] in simulation. **A)** Overlay of the RMSF plots of isomer **A** (black), isomer **A** with the in silico

removal of the *in silico* removal of the C_{19}-C_{25} disulfide bond (blue) and the analog $A_{[C19S,C25S]}$. **B)** 100 snapshots from the 300 ns MD simulation of $A_{[C19S,C25S]}$ showing its conformational flexibility shown by the orange curve in the plot to its left. **C)** Overlay of the RMSF plots of isomer **B** (black), isomer **B** with the in silico removal of the *in silico* removal of the C_{19}-C_{25} disulfide bond (blue) and the analog $B_{[C19S,C25S]}$. **D)** 100 snapshots from the 300 ns MD simulation of $B_{[C19S,C25S]}$ showing its conformational flexibility shown by the orange curve in the plot to its left. **E)** Overlay of the RMSF plots of isomer **C** (black), isomer **C** with the in silico removal of the *in silico* removal of the C_{19}-C_{25} disulfide bond (blue) and the analog $C_{[C19S,C25S]}$. **F)** 100 snapshots from the 300 ns MD simulation of $C_{[C19S,C25S]}$ showing its conformational flexibility shown by the orange curve in the plot to its left.

Supporting text

Molecular dynamics based analysis of the conformational dynamics of tridegin isomers

Isomer **A** showed a moderate level of inherent flexibility of 3.33 Å backbone RMSD for the whole molecule. The disulfide linked part of the peptide (residues 1-37) had a RMSD of 2.36 Å and the C-terminal segment comprising of residues 38-66 depicted a 3.94 Å backbone RMSD contribution (Table S8, Figure S10). Upon removal of the C_{19}-C_{25} disulfide bond, the overall backbone RMSD took a slight dip to 2.80 Å. The main reason for this is the marginal gain of backbone rigidity due to the formation of intramolecular hydrogen bonds by the free thiol groups of the reduced cysteines. This is a consequence of favorable reorientations of the side chain residues of the cysteines as well as other residues in the vicinity. The replacement of cysteines C_{19} and C_{25} by serines brought the overall peptide flexibility down to 2.59 Å. However, the flexibility of the C-terminal region between residues 38 and 66 increased from 2.60 Å to 2.93 Å.

For the disulfide deficient version of isomer **B** the backbone RMSD showed a slight increase from 2.70 Å for the **B** variant to 3.10 Å. 100 conformations sampled by this peptide from uniform intervals of the simulation trajectory are superimposed with the regions of flexibility highlighted in Figures S12 C. The flexibility of the region between residues 38 and 66 in comparison to the disulfide linked part of the peptide is shown in Figure S12 C, D. The largest amount of flexibility observed among all three isomers was for the serine mutated version **B[C19S,C25S]**. The overall backbone RMSD was 10.75 Å with the greatest contributor to this extreme structural deviation arising from the C-terminal region (residues 38 to 66) with an RMSD contribution of 8.25 Å. The disulfide-linked part of the peptide (residues 1 to 37) on the other hand, remained unhinged with a meagre 1.54 Å backbone RMSD.

The isomer that displayed the greatest amount of structural rigidity was the wild type variant of isomer **C**. With a backbone RMSD of 1.71 Å, the entire molecule including the C-terminal region remained structurally rigid (Figure S12 E). This could be attributed to the constrained conformation rendered by the disulfide bridging between C_5-C_{37} and C_{17}-C_{31}. This has further consequences by allowing formation of stable hydrogen bonds between the otherwise flexible C-terminal region and the disulfide bound region of the peptide. Resulting hydrogen bonding was observed between L_2 and L_3 to G_{56}, K_{45} to D_{49}, D_{48} to R_{53}, and Y_{51} to A_{26}. The C-terminal region remains almost wrapped around the disulfide-bound region of the peptide through the entire course of the simulation (Figure S12). The opening of the C_{19}-C_{25} disulfide bond caused moderate increase in backbone RMSD while the RMSD of the C-terminal part fell lower (from 1.68 Å in the parent type) to 1.62 Å. The structural constraint enforced by the remaining two disulfide bonds, in particular along with the hydrophobicity induced by the presence of the unbound cysteines, keeps the entire peptide in a relatively immobile conformation. All of the hydrogen bonds that were present in the isomer **C** were found in the disulfide-deficient variant as well. This observed conformation of the peptide including the C-terminal region could be the reason as to why this isomer chose to bind in a different part of FXIIIa as found in previous studies.[1] The substitution of the C_{19} and C_{25} by serines caused a dramatic structural deviation of the isomer. The overall backbone RMSD with respect to its starting structure increased to 7.03 Å with the lion's share of it coming from the C-terminal region (6.52 Å). Table S8 lists the individual backbone RMSD values for each isomer along with the individual contributions of the N-terminal (residues 1-37) and C-terminal (residues 38-66) regions of the peptide. The atoms C, Cα, N and O were taken into consideration for the computation of backbone RMSD.

In all of the isomers handled in this study, despite large initial deviations from the starting conformations especially by the conformations sampled between residues 38-66 (Figure S9), extended equilibration simulations (300 ns simulations) indicate that all structures reach a well-equilibrated conformational ensemble with the RMSD in the range of 2 Å (Figures S10, S11).

Since the RMSD values obtained for individual isomers while considering the entire molecule were affected by distinct regions of the peptide with high flexibility, these regions of the peptide were identified and compared among the variants of the isomer (Figure S12 and S14). As a natural consequence of introducing additional flexibility by computationally opening disulfide bonds, these variants have an increase in conformational flexibility as indicated by the per-residue RMSF plots in Figure S9, S12, and S14.

Similar effects in the novel analogs ($\mathbf{A_{[C19S,C25S]}}$, $\mathbf{B_{[C19S,C25S]}}$, $\mathbf{C_{[C19S,C25S]}}$) can also be attributed to the loss of disulfide-bond induced constraint and the alteration of hydrophobicity due to the serine mutations. This is based on the fact that cysteine has a much larger hydrophobic surface area of 119 $Å^2$ as opposed to serine with only 36 $Å^2$ as reported by Lins et al.[2] A large amount of structural flexibility arises from the disordered C-terminal domain (residues 38-66), which makes up ~ 43% of the sequence. Although this results in numerically higher average global RMSD values ranging from 1.62 Å to 8.25 Å (average of 3.8 Å), this is an inherent property of these peptides and also a phenomenon observed in similar leech-derived peptides belonging to the hirudin family.[3] This is further highlighted by the RMSF values of the disordered C-terminal domain (residues 38-66) being much higher than the RMSF values for the rest of the sequence (Table S8 and Figure S9 D, E, F).

To aid further understanding into the effect of the *in silico* removal of the C_{19}-C_{25} disulfide bonds on the structural evolution, the distances sampled by these unbound cysteine residues

during simulation were observed and plotted (Figure S13). As demonstrated earlier, this approach helps to determine the dependence of the peptide on a particular disulfide bond to maintain structural integrity.[4] The distance vs. simulation time plots indicate that the S_γ atoms (red curves in Figure S11) of the unbound C_{19} and C_{25} residues stay within proximities of their initial conformation at multiple instances within 300 ns of simulation time. This is an indication that the opening of this C_{19}-C_{25} disulfide bond does not promote unfolding or structural disruption of the peptide. This observation is consistent between all the three isomers although in isomer **C** (Figure S13) the S_γ atoms tend to move the farthest away from each other between 150 and 180 ns of the simulation before falling back to initial distances. The distances between the C_α atoms of residues C_{19} and C_{25} indicated by the black traces in Figure S13 show the extent the backbone is affected by the opening of the disulfide bond. It further tries to build a relationship between the unbound S_γ mobility and the extent backbone deviation indicated by the C_α distances. We can safely conclude that for isomers **A** and **B** the removal of the C_{19}-C_{25} disulfide bond has very little effect on its backbone indicated by a relatively unwavering black curve (Figure S13) representing the C_α proximity between the unbound cysteines. In the case of isomer **C**, the movement of the backbone is to a good extent governed by the movement of the unbound cysteine residues and, interestingly, seems to have a direct correlation with the RMSD progression of the C-terminal segment of this isomer (Figure S13). The conformational ensembles of the serine mutated analogs are presented in Figure S14 along with comparative RMSF plots.

Turbidity assay

   Clotting assays were performed immediately after NPP was thawed at 37 ºC. NPP was combined with Tridegin variant or HEPES-buffered saline (20 mM HEPES pH 7.4, 150 mM NaCl; HBS). Clotting was initiated by incubating recalcified (10 mM $CaCl_2$, final) NPP with tissue factor and phospholipids (1:12,000 dilution of Innovin and 4 µM, final, respectively) in a 96-well flat-bottom plate. Final reaction volumes were 100 µL (80% NPP). Clot formation was monitored by turbidity at 405 nm for 1.5 hours (SpectraMax 384Plus plate reader, Molecular Devices, Sunnyvale, CA) at room temperature.

REFERENCES

(1)   Böhm, M.; Bäuml, C. A.; Hardes, K.; Steinmetzer, T.; Roeser, D.; Schaub, Y.; Than, M.
E.; Biswas, A.; Imhof, D. Novel Insights into Structure and Function of Factor XIIIa-
Inhibitor Tridegin. *J. Med. Chem.* **2014**, *57*, 10355–10365.

(2)   Lins, L.; Thomas, A.; Brasseur, R. Analysis of Accessible Surface of Residues in Proteins.
Protein Sci. **2003**, *12*, 1406–1417.

(3)   Huang, Y.; Zhang, Y.; Zhao, B.; Xu, Q.; Zhou, X.; Song, H.; Yu, M.; Mo, W. Structural
Basis of RGD-Hirudin Binding to Thrombin: Tyr3and Five C-Terminal Residues Are
Crucial for Inhibiting Thrombin Activity. *BMC Struct. Biol.* **2014**, *14*, 26.

(4)   Paul George, A. A.; Heimer, P.; Maaß, A.; Hamaekers, J.; Hofmann-Apitius, M.; Biswas,
A.; Imhof, D. Insights into the Folding of Disulfide-Rich μ-Conotoxins. *ACS Omega*
2018, *3*, 12330–12340.